

Object Detection and Pose Estimation from RGB and Depth Data for Real-time, Adaptive Robotic Grasping

Shuvo Kumar Paul¹, Muhammed Tawfiq Chowdhury¹, Mircea Nicolescu¹, Monica Nicolescu¹, David Feil-Seifer¹

Abstract—In recent times, object detection and pose estimation have gained significant attention in the context of robotic vision applications. Both the identification of objects of interest as well as the estimation of their pose remain important capabilities in order for robots to provide effective assistance for numerous robotic applications ranging from household tasks to industrial manipulation. This problem is particularly challenging because of the heterogeneity of objects having different and potentially complex shapes, and the difficulties arising due to background clutter and partial occlusions between objects. As the main contribution of this work, we propose a system that performs real-time object detection and pose estimation, for the purpose of dynamic robot grasping. The robot has been pre-trained to perform a small set of canonical grasps from a few fixed poses for each object. When presented with an unknown object in an arbitrary pose, the proposed approach allows the robot to detect the object identity and its actual pose, and then adapt a canonical grasp in order to be used with the new pose. For training, the system defines a canonical grasp by capturing the relative pose of an object with respect to the gripper attached to the robot's wrist. During testing, once a new pose is detected, a canonical grasp for the object is identified and then dynamically adapted by adjusting the robot arm's joint angles, so that the gripper can grasp the object in its new pose. We conducted experiments using a humanoid PR2 robot and showed that the proposed framework can detect well-textured objects, and provide accurate pose estimation in the presence of tolerable amounts of out-of-plane rotation. The performance is also illustrated by the robot successfully grasping objects from a wide range of arbitrary poses.

Index Terms—pose estimation, robotics, robotic grasp, homography

I. INTRODUCTION

Current advances in robotics and autonomous systems have expanded the use of robots in a wide range of robotic tasks including assembly, advanced manufacturing, human-robot or robot-robot collaboration. In order for robots to efficiently perform these tasks, they need to have the ability to adapt

to the changing environment while interacting with their surroundings, and a key component of this interaction is the reliable grasping of arbitrary objects. Consequently, a recent trend in robotics research has focused on object detection and pose estimation for the purpose of dynamic robotic grasping.

However, identifying objects and recovering their poses are particularly challenging tasks as objects in the real world are extremely varied in shape and appearance. Moreover, cluttered scenes, occlusion between objects, and variance in lighting conditions make it even more difficult. Additionally, the system needs to be sufficiently fast to facilitate real-time robotic tasks. As a result, a generic solution that can address all these problems remains an open challenge.

While classification [1–6], detection [7–12], and segmentation [13–15] of objects from images have taken a significant step forward - thanks to deep learning, the same has not yet happened to 3D localization and pose estimation. One primary reason was the lack of labeled data in the past as it is not practical to manually infer, thus As a result, the recent research trend in the deep learning community for such applications has shifted towards synthetic datasets [16–20]. Several pose estimation methods leveraging deep learning techniques [21–25] use these synthetic datasets for training and have shown satisfactory accuracy.

Although synthetic data is a promising alternative, capable of generating large amounts of labeled data, it requires photo-realistic 3D models of the objects to mirror the real-world scenario. Hence, generating synthetic data for each newly introduced object needs photo-realistic 3D models and thus significant effort from skilled 3D artists. Furthermore, training and running deep learning models are not feasible without high computing resources as well. As a result, object detection and pose estimation in real-time with computationally moderate machines remain a challenging problem. To address these issues, we have devised a simpler pipeline that does not rely on high computing resources and focuses on planar objects, requiring only an RGB image and the depth information in order to infer real-time object detection and pose estimation.

In this work, we present a feature-detector-descriptor based method for detection and a homography based pose estimation technique where, by utilizing the depth information, we estimate the pose of an object in terms of a 2D planar representation in 3D space. The robot is pre-trained to perform

^{*}This work has been supported in part by the Office of Naval Research award N00014-16-1-2312 and US Army Research Laboratory (ARO) award W911NF-20-2-0084.

¹**Contact author:** Shuvo Kumar Paul, Muhammed Tawfiq Chowdhury, Mircea Nicolescu, Monica Nicolescu, and David Feil-Seifer are affiliated with the Department of Computer Science and Engineering, University of Nevada, Reno, 1664 North Virginia Street, Reno, Nevada 89557, USA shuvo.k.paul@nevada.unr.edu, mtawfiq@nevada.unr.edu, mircea@cse.unr.edu, monica@cse.unr.edu, dave@cse.unr.edu

a set of canonical grasps; a canonical grasp describes how a robotic end-effector should be placed relative to an object in a fixed pose so that it can securely grasp it. Afterward, the robot is able to detect objects and estimates their pose in real-time, and then adapt the pre-trained canonical grasp to the new pose of the object of interest. We demonstrate that the proposed method can detect a well-textured planar object and estimate its accurate pose within a tolerable amount of out-of-plane rotation. We also conducted experiments with the humanoid PR2 robot to show the applicability of the framework where the robot grasped objects by adapting to a range of different poses.

II. RELATED WORK

Our work constitutes of three modules: object detection, planar pose estimation, and adaptive grasping. In the following sub-sections, several fields of research that are closely related to our work are reviewed.

A. Object Detection

Object detection has been one of the fundamental challenges in the field of computer vision and in that aspect, the introduction of feature detectors and descriptors represents a great achievement. Over the past decades, many detectors, descriptors, and their numerous variants have been presented in the literature. The applications of these methods have widely extended to numerous other vision applications such as panorama stitching, tracking, visual navigation, etc.

One of the first feature detectors was proposed by Harris et al. [26] (widely known as the Harris corner detector). Later Tomasi et al. [27] developed the KLT (Kanade-Lucas-Tomasi) tracker based on the Harris corner detector. Shi and Tomasi introduced a new detection metric GFTT [28] (Good Features To Track) and argued that it offered superior performance. Hall et al. introduced the concept of saliency [29] in terms of the change in scale and evaluated the Harris method proposed in [30] and the Harris Laplacian corner detector [31] where a Harris detector and a Laplacian function are combined.

Motivated by the need for a scale-invariant feature detector, in 2004 Lowe [32] published one of the most influential papers in computer vision, SIFT (Scale Invariant Feature Transform). SIFT is both a feature point detector and descriptor. H. Bay et al. [33] proposed SURF (Speeded Up Robust Features) in 2008. But both of these methods are computationally expensive as SIFT detector leverages the difference of Gaussians (DoG) in different scales while SURF detector uses a Haar wavelet approximation of the determinant of the Hessian matrix to speed up the detection process. Many variants of SIFT [34–37] and SURF [38–40] were proposed, either targeting a different problem or reporting improvements in matching, however, the execution time remained a persisting problem for several vision applications.

To improve execution time, several other detectors such as FAST [41] and AGAST [42] have been introduced. Calonder et al. developed the BRIEF [43] (Binary Robust Independent Elementary Features) descriptor of binary strings that has a

fast execution time and is very useful for matching images. E. Rublee et al. presented ORB [44] (Oriented FAST and Rotated Brief) which is a combination of modified FAST (Features from Accelerated Segment Test) for feature detection and BRIEF for description. S. Leutnegger et al. designed BRISK [45] (Binary Robust Invariant Scale Keypoint) that detects corners using AGAST and filters them using FAST. On the other hand, FREAK (Fast Retina Key-point), introduced by Alahi et al. [46] generates retinal sampling patterns using a circular sampling grid and uses a binary descriptor, formed by a one bit difference of Gaussians (DoG). Alcantarilla et al. introduced KAZE [47] features that exploit non-linear scale-space using non-linear diffusion filtering and later extended it to AKAZE [48] where they replaced it with a more computationally efficient method called FED (Fast Explicit Diffusion) [49, 50].

In our work, we have selected four methods to investigate: SIFT, SURF, FAST+BRISK, AKAZE.

B. Planar Pose Estimation

Among the many techniques in literature on pose estimation, we focus our review on those related to planar pose estimation. In recent years, planar pose estimation has been increasingly becoming popular in many fields, such as robotics and augmented reality.

Simon et. al [51] proposed a pose estimation technique for planar structures using homography projection and by computing camera pose from consecutive images. Changhai et. al [52] presented a method to robustly estimate 3D poses of planes by applying a weighted incremental normal estimation method that uses Bayesian inference. Donoser et al. [53] utilized the properties of Maximally Stable Extremal Regions (MSERs [54]) to construct a perspective invariant frame on the closed contour to estimate the planar pose. In our approach, we applied perspective transformation to approximate a set of corresponding points on the test image for estimating the basis vectors of the object surface and used the depth information to estimate the 3D pose by computing the normal to the planar object.

C. Adaptive Grasping

Designing an adaptive grasping system is challenging due to the complex nature of the shapes of objects. In early times, analytical methods were used where the system would analyze the geometric structure of the object and would try to predict suitable grasping points. Sahbani et al. [55] did an in depth review on the existing analytical approaches for 3D object grasping. However, with the analytical approach it is difficult to compute force and not suitable for autonomous manipulation. Later, as the number of 3D models increased, numerous data driven methods were introduced that would analyze grasps in the 3D model database and then transfer to the target object. Bohg et al. [56] reviewed data driven grasping method methods where they divided the approach into three groups based on the familiarity of the object.

Kehoe et al. [57] used a candidate grasp from the candidate grasp set based on the feasibility score determined by the grasp planner. The grasps weren't very accurate in situations where the objects had stable horizontal poses and were close to the width of the robot's gripper. Huebner et al. [58] also take a similar approach as they perform grasp candidate simulation. They created a sequence of grasps by approximating the shape of the objects and then computed a random grasp evaluation for each model of objects. In both works, a grasp has been chosen from a list of candidate grasps.

The recent advances in deep learning also made it possible to regress grasp configuration through deep convolutional networks. A number of deep learning-based methods were reviewed in [59] where the authors also discussed how each element in deep learning-based methods enhances the robotic grasping detection. [60] presented a system where deep neural networks were used to learn hierarchical features to detect and estimate the pose of an object, and then use the centers of the defined pose classes to grasp the objects. Kroemer et al. [61] introduced an active learning approach where the robot observes a few good grasps by demonstration and learns a value function for these grasps using Gaussian process regression. Aleotti et al. [62] proposed a grasping model that is capable of grasping objects by their parts which learns new tasks from human demonstration with automatic 3D shape segmentation for object recognition and semantic modeling. [63] and [64] used supervised learning to predict grasp locations from RGB images. In [65], as an alternative to a trial and error exploration strategy, the authors proposed a Bayesian optimization technique to address the robot grasp optimization problem of unknown objects. These methods emphasized developing and using learning models for obtaining accurate grasps.

In our work, we focus on pre-defining a suitable grasp relative to an object that can adapt to a new grasp based on the change of position and orientation of the object.

III. METHOD

The proposed method is divided into two parts. The first part outlines the process of simultaneous object detection and pose estimation of multiple objects and the second part describes the process of generating an adaptive grasp using the pre-trained canonical grasp and the object pose. The following sections describe the architecture of the proposed framework (figure 2) in detail.

A. Object Detection and Pose Estimation

We present a planar pose estimation algorithm (algorithm 1) for adaptive grasping that consists of four phases: (i) feature extraction and matching, (ii) homography estimation and perspective transformation, (iii) directional vectors estimation on the object surface, (iv) planar pose estimation using the depth data. In the following sections, we will focus on the detailed description of the aforementioned steps.

1) *Feature extraction and matching*: Our object detection starts with extracting features from the images of the planar objects and then matching them with the features found in the

images acquired from the camera. Image features are patterns in images based on which we can describe the image. A feature detecting algorithm takes an image and returns the locations of these patterns - they can be edges, corners or interest points, blobs or regions of interest points, ridges, etc. This feature information then needs to be transformed into a vector space using a feature descriptor, so that it gives us the possibility to execute numerical operations on them. A feature descriptor encodes these patterns into a series of numerical values that can be used to match, compare, and differentiate one feature to another; for example, we can use these feature vectors to find the similarities in different images which can lead us to detect objects in the image. In theory, this information would be invariant to image transformations. In our work, we have investigated SIFT [32], SURF [33], AKAZE [48], and BRISK [45] descriptors. SIFT, SURF, AKAZE are both feature detectors and descriptors, but BRISK uses FAST [41] algorithm for feature detection. These descriptors were selected after carefully reviewing the comparisons done in the recent literature [66–68].

Once the features are extracted and transformed into vectors, we compare the features to determine the presence of an object in the scene. For non-binary feature descriptors (SIFT, SURF) we find matches using the Nearest Neighbor algorithm. However, finding the nearest neighbor matches within high dimensional data is computationally expensive, and with more objects introduced it can affect the process of updating the pose in real-time. To counter this issue to some extent, we used the FLANN [69] implementation of K-d Nearest Neighbor Search, which is an approximation of the K-Nearest Neighbor algorithm that is optimized for high dimensional features. For binary features (AKAZE, BRISK), we used the Hamming distance ratio method to find the matches. Finally, if we have more than ten matches, we presume the object is present in the scene.

2) *Homography Estimation and Perspective Transformation*: A homography is an invertible mapping of points and lines on the projective plane that describes a 2D planar projective transformation (figure 1) that can be estimated from a given pair of images. In simple terms, a homography is a matrix that maps a set of points in one image to the corresponding set of points in another image. We can use a homography matrix \mathbf{H} to find the corresponding points using equation 1 and 2, which defines the relation of projected point (x', y') (figure 1) on the rotated plane to the reference point (x, y) .

A 2D point (x, y) in an image can be represented as a 3D vector $(x, y, 1)$ which is called the homogeneous representation of a point that lies on the reference plane or image of the planar object. In equation (1), \mathbf{H} represents the homography matrix and $[x \ y \ 1]^T$ is the homogeneous representation of the reference point (x, y) and we can use the values of a, b, c to estimate the projected point (x', y') in equation (2).

Algorithm 1: Planar Pose Estimation

```

Input: Training images of planar objects,  $\mathcal{I}$ 
1  $Detector \leftarrow$  Define feature detector
2  $Descriptor \leftarrow$  Define feature descriptor
3 /* retrieve feature descriptor */
4 /* for each image in  $\mathcal{I}$  */
5 for  $i$  in  $\mathcal{I}$  do
6   /*  $\mathcal{K}$  is set of detected keypoints for image  $i$  */
7    $\mathcal{K} \leftarrow \text{DetectKeypoints}(i, Detector)$ 
8   /*  $\mathcal{D}[i]$  is the corresponding descriptor set for image  $i$  */
9    $\mathcal{D}[i] \leftarrow \text{GetDescriptors}(\mathcal{K}, Descriptor)$ 
10 end for
11 while camera is on do
12    $f \leftarrow$  RGB image frame
13    $PC \leftarrow$  Point cloud data
14   /*  $\mathcal{K}_F$  is set of detected keypoints for image frame  $f$  */
15    $\mathcal{K}_F \leftarrow \text{DetectKeypoints}(f, Detector)$ 
16   /*  $\mathcal{D}_F$  is the corresponding descriptor set for rgb image  $f$  */
17    $\mathcal{D}_F \leftarrow \text{GetDescriptors}(\mathcal{K}_F, Descriptor)$ 
18   for  $i$  in  $\mathcal{I}$  do
19      $matches \leftarrow \text{FindMatches}(\mathcal{D}[i], \mathcal{D}_F)$ 
20     /* If there is at least 10 matches then we have the object (described in image  $i$ ) in the scene */
21     if Total number of matches  $\geq 10$  then
22       /* extract matched keypoints pair  $(kp_i, kp_f)$  from the corresponding descriptors matches. */
23        $kp_i, kp_f \leftarrow \text{ExtractKeypoints}(matches)$ 
24        $\mathbf{H} \leftarrow \text{EstimateHomography}(kp_i, kp_f)$ 
25        $p_c, p_x, p_y \leftarrow$  points on the planar object obtained using equation (3)
26        $p'_c, p'_x, p'_y \leftarrow$  corresponding projected points of  $p_c, p_x, p_y$  on image frame  $f$  estimated using equations (1) and (2)
27       /*  $\vec{c}$  denotes the origin of the object frame with respect to the base/world frame */
28        $\vec{c}, \vec{x}, \vec{y} \leftarrow$  corresponding 3d locations of  $p'_c, p'_x, p'_y$  from point cloud  $PC$ 
29       /* shift  $\vec{x}, \vec{y}$  to the origin of the base or the world frame */
30        $\vec{x} \leftarrow \vec{x} - \vec{c}$ 
31        $\vec{y} \leftarrow \vec{y} - \vec{c}$ 
32       /* estimate the object frame in terms of three orthonormal vectors  $\hat{i}, \hat{j}$ , and  $\hat{k}$ . */
33        $\hat{i}, \hat{j}, \hat{k} \leftarrow$  from equation (4)
34       /* compute the rotation  $\phi_i, \theta_i, \psi_i$  of the object frame  $\hat{i}, \hat{j}, \hat{k}$  with respect to the base or the world frame  $\vec{X}, \vec{Y}, \vec{Z}$ . */
35        $\phi_i, \theta_i, \psi_i \leftarrow$  from equation (8)
36       /* finally, publish the position and orientation of the object. */
37       publish( $\vec{c}, \phi_i, \theta_i, \psi_i$ )
38   end for
39 end while

```

$$\begin{bmatrix} a \\ b \\ c \end{bmatrix} = \mathbf{H} \begin{bmatrix} x \\ y \\ 1 \end{bmatrix} = \begin{bmatrix} h_{11} & h_{12} & h_{13} \\ h_{21} & h_{22} & h_{23} \\ h_{31} & h_{32} & h_{33} \end{bmatrix} \begin{bmatrix} x \\ y \\ 1 \end{bmatrix} \quad (1)$$

$$\begin{cases} x' = \frac{a}{c} \\ y' = \frac{b}{c} \end{cases} \quad (2)$$

We estimate the homography using the matches found from the nearest neighbor search as input; often these matches can have completely false correspondences, meaning they don't correspond to the same real-world feature at all which can be a problem in estimating the homography. So, we chose

RANSAC [70] to robustly estimate the homography by considering only inlier matches as it tries to estimate the underlying model parameters and detect outliers by generating candidate solutions through random sampling using a minimum number of observations.

While the other techniques use as much data as possible to find the model parameters and then pruning the outliers, RANSAC uses the smallest set of data point possible to estimate the model, thus making it faster and more efficient than the conventional solutions.

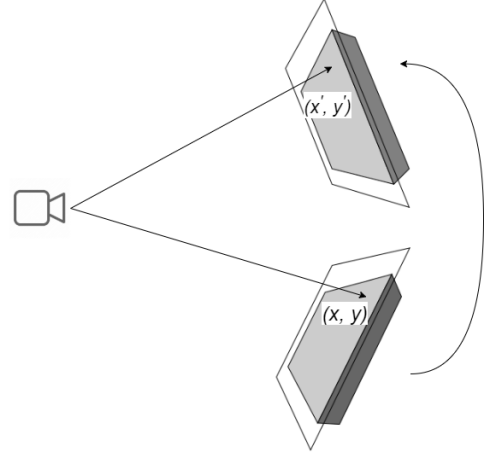


Fig. 1: Object in different orientation from the camera

3) *Finding directional vectors on the object:* In order to find the pose of a planar object, we need to find the three orthonormal vectors on the planar object that describe the object coordinate frame and consequently, the orientation of the object relative to the world coordinate system. We start by estimating the vectors on the planar object that form the basis of the plane, illustrated in figure 3. Then, we take the cross product of these two vectors to find the third directional vector which is the normal to the object surface. Let's denote the world coordinate system as XYZ , and the object coordinate system as xyz . We define the axes of the orientation in relation to a body as:

$x \rightarrow$ right
 $y \rightarrow$ up
 $z \rightarrow$ towards the camera

First, we retrieve the locations of the three points p_c, p_x, p_y on the planar object from the reference image using equation (3) and then locate the corresponding points p'_c, p'_x, p'_y on the image acquired from the Microsoft Kinect sensor. We estimate the locations of these points using the homography matrix \mathbf{H} as shown in equation 1, 2. Then we find the corresponding 3D locations of p_c, p_x, p_y from the point cloud data also obtained from the Microsoft Kinect sensor. We denote them as vectors \vec{c}, \vec{x} , and \vec{y} . Here, \vec{c} represents the translation vector from the object frame to the world frame and also the position of the object in the world frame. Next, we subtract \vec{c} from \vec{x}, \vec{y} which essentially gives us two vectors \vec{x} and \vec{y} centered at

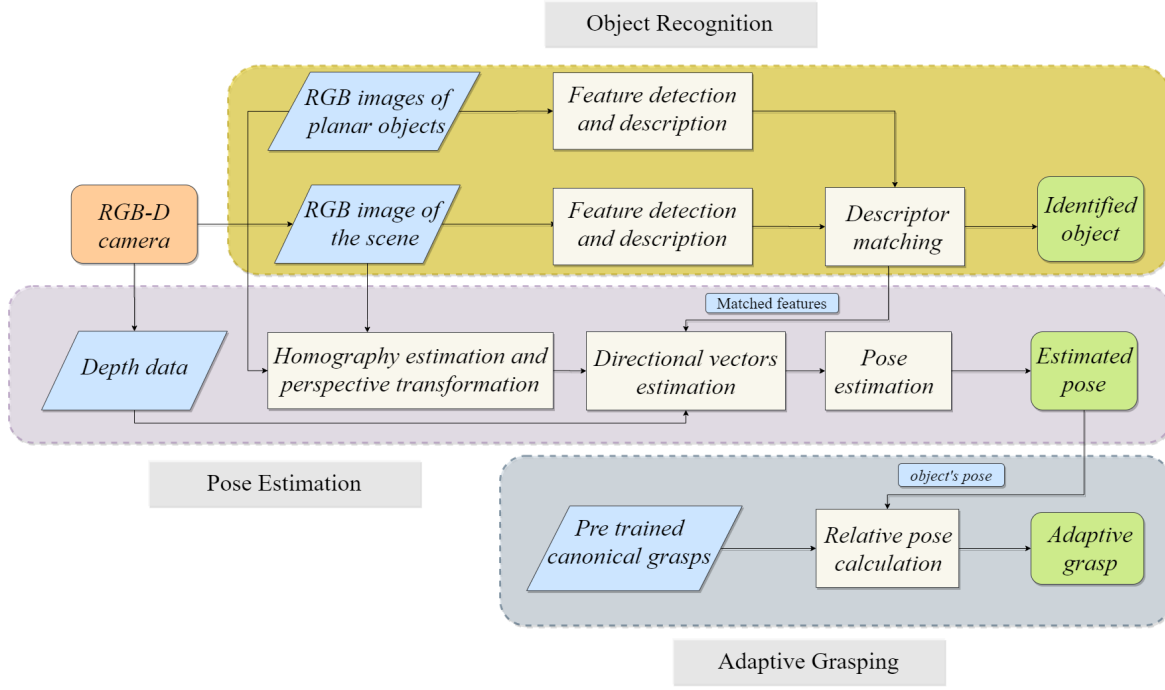


Fig. 2: System architecture.

the origin of the world frame. We take the cross product of these two vectors \vec{x}, \vec{y} to find the third axis \vec{z} . But, depending on the homography matrix the estimated axes \vec{x} and \vec{y} might not be exactly orthogonal, so we take the cross product of \vec{y} and \vec{z} to recalculate the vector \vec{x} . Now that we have three orthogonal vectors, we compute the three unit vectors \hat{i}, \hat{j} , and \hat{k} along the \vec{x}, \vec{y} , and \vec{z} vectors respectively using equation 4. These three orthonormal vectors describe the object frame. These vectors were projected onto the image plane to give a visual confirmation of the methods applied; figure 4 shows the orthogonal axes projected onto the object plane.

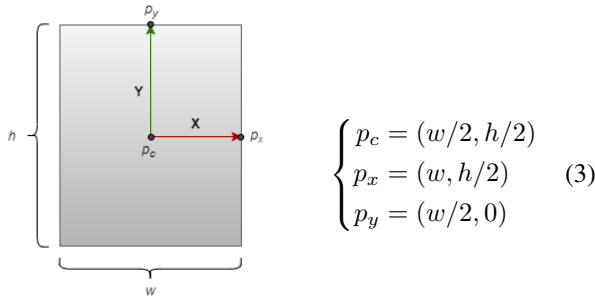


Fig. 3: Axis on the reference plane

$$\begin{aligned} \hat{j} &= \frac{\vec{y}}{|\vec{y}|} = [j_X \ j_Y \ j_Z] \\ \hat{k} &= \frac{\vec{x} \times \vec{y}}{|\vec{x} \times \vec{y}|} = [k_X \ k_Y \ k_Z] \\ \hat{i} &= \frac{\vec{y} \times \vec{z}}{|\vec{y} \times \vec{z}|} = [i_X \ i_Y \ i_Z] \end{aligned} \quad (4)$$



Fig. 4: Computed third directional axis projected onto image plane

4) *Planar pose computation*: We compute the pose of the object in terms of the Euler angles. Euler angles are three angles that describe the orientation of a rigid body with respect to a fixed coordinate system. The rotation matrix \mathbf{R} in equation (5) rotates X axis to \hat{i} , Y axis to \hat{j} , and Z axis to \hat{k} .

$$\mathbf{R} = \begin{bmatrix} i_X & j_X & k_X \\ i_Y & j_Y & k_Y \\ i_Z & j_Z & k_Z \end{bmatrix} \quad (5)$$

Euler angles are combinations of the three axis rotations (equation 6), where ϕ , θ , and ψ specify the intrinsic rotations around the X, Y, and Z axis respectively. The combined rotation matrix is a product of three matrices: $\mathbf{R} = \mathbf{R}_z \mathbf{R}_y \mathbf{R}_x$ (equation 7); the first intrinsic rotation rightmost, last leftmost.

$$\begin{cases} \mathbf{R}_x = \begin{bmatrix} 1 & 0 & 0 \\ 0 & \cos \phi & -\sin \phi \\ 0 & \sin \phi & \cos \phi \end{bmatrix} \\ \mathbf{R}_y = \begin{bmatrix} \cos \theta & 0 & \sin \theta \\ 0 & 1 & 0 \\ -\sin \theta & 0 & \cos \theta \end{bmatrix} \\ \mathbf{R}_z = \begin{bmatrix} \cos \psi & -\sin \psi & 0 \\ \sin \psi & \cos \psi & 0 \\ 0 & 0 & 1 \end{bmatrix} \end{cases} \quad (6)$$

$$\mathbf{R} = \begin{bmatrix} c\theta c\psi & s\phi s\theta c\psi - c\phi s\psi & c\phi s\theta c\psi + s\phi s\psi \\ c\theta s\psi & s\phi s\theta s\psi + c\phi c\psi & c\phi s\theta s\psi - s\phi c\psi \\ -s\theta & s\phi c\theta & c\phi c\theta \end{bmatrix} \quad (7)$$

In equation 7, c and s represents \cos and \sin respectively. Solving for ϕ, θ , and ψ from (5) and (7), we get,

$$\begin{cases} \phi = \tan^{-1} \left(\frac{j_Z}{k_Z} \right) \\ \theta = \tan^{-1} \left(\frac{-i_Z}{\sqrt{1 - i_Z^2}} \right) = \sin^{-1}(-i_Z) \\ \psi = \tan^{-1} \left(\frac{i_Y}{i_X} \right) \end{cases} \quad (8)$$

B. Training Grasps for Humanoid Robots

To ensure that the robot can grasp objects in an adaptive manner, we pre-train the robot to perform a set of canonical grasps. We place the object and the robot's gripper close to each other and record the relative pose. This essentially gives us the pose of the gripper with respect to the object. Figure 6 illustrates the training process in which the robot's gripper and a cracker box have been placed in close proximity and the relative poses have been recorded for grasping the objects from the side.

$$\mathbf{T}_s^d = \begin{bmatrix} \mathbf{R}_s^d & P_s^d \\ 0 & 1 \end{bmatrix} = \begin{bmatrix} r_{11} & r_{12} & r_{13} & X_t \\ r_{21} & r_{22} & r_{23} & Y_t \\ r_{31} & r_{32} & r_{33} & Z_t \\ 0 & 0 & 0 & 1 \end{bmatrix} \quad (9)$$

Equation 9 outlines the structure of a transformation matrix \mathbf{T}_s^d that describes the rotation and translation of frame d with respect to frame s ; \mathbf{R}_s^d represents the rotation matrix similar to equation 7 and $P_s^d = [X_t, Y_t, Z_t]^T$ is the translation matrix which is the 3D location of the origin of frame d in frame s .

During the training phase, we first formulate the transformation matrix \mathbf{T}_b^o using the rotation matrix and the object location. We take the inverse of \mathbf{T}_b^o which gives us the transformation matrix \mathbf{T}_o^b . We then use the equation 10 to record the transformation \mathbf{T}_o^g of the robot's wrist relative to the object.

$$\mathbf{T}_o^g = \mathbf{T}_o^b \times \mathbf{T}_b^g \text{ where } \mathbf{T}_o^b = (\mathbf{T}_b^o)^{-1} \quad (10)$$

In the equation 10, b refers to the robot's base, o refers to the object, and g refers to the wrist of the robot to which the gripper is attached. Once we record the matrix, we get a new pose of the object from the vision in the testing phase and generate the final matrix using the equation 11 that has the new position and orientation of the robot's wrist in matrix form .

$$\mathbf{T}_b^g = \mathbf{T}_b^o \times \mathbf{T}_o^g \quad (11)$$

We then extract the rotational angles γ, β, α (roll, pitch, yaw) of the grasp pose from matrix \mathbf{T}_b^g using equation 12

$$\begin{cases} \gamma = \tan^{-1}(r_{32}/r_{33}) \\ \beta = \tan^{-1} \frac{-r_{31}}{\sqrt{r_{32}^2 + r_{33}^2}} \\ \alpha = \tan^{-1}(r_{21}/r_{11}) \end{cases} \quad (12)$$

IV. EVALUATION

The proposed object recognition and pose estimation algorithm was implemented on an Ubuntu 14.04 platform equipped with 3.0 GHz Intel R Core(TM) i5-7400 CPU and 8GB system memory. The RGB-D camera used in the experiments was a Microsoft Kinect sensor v1. We evaluated the proposed algorithm by comparing the accuracy of object recognition, pose estimation, and execution time of four different feature descriptors. We also validated the effectiveness of our approach for adaptive grasping by conducting experiments with the PR2 robot.

A. Object detection and pose estimation

Without enough observable features, the system would fail to find good matches that are required for accurate homography estimation. Consequently, our object detection and pose estimation approach has a constraint on the out-of-plane rotation θ , illustrated in figure 7. In other words, if the out-of-plane rotation of the object is more than θ , the system would not be able to recognize the object. Fast execution is also a crucial aspect to facilitate multiple object detection and pose estimation for real-time applications. We experimented with four different descriptors on several planar objects and the comparative result is shown in table I. The execution time was measured for the object detection and pose estimation step. AKAZE and BRISK had much lower processing time for detection and pose estimation, thus would have a better frame rate, but SIFT and SURF had larger out-of-plane rotational freedom.

TABLE I: Comparison of feature descriptors

Descriptor	Maximum out of plane rotation (degree)	Execution time (second)
SIFT	$48^\circ \pm 2^\circ$	0.21s
SURF	$37^\circ \pm 2^\circ$	0.27s
AKAZE	$18^\circ \pm 1^\circ$	0.05s
BRISK	$22^\circ \pm 2^\circ$	0.06s

We also compared the *RMS* difference ϵ (equation 13) of re-calculated \vec{x} to original \vec{x} (\vec{x}' in the equation) for increasing out-of-plane rotation of the planar objects to assess the homography estimation. Ideally, the two estimated vectors \vec{x} and \vec{y} , which describe the basis of the plane of the planar object, should be orthogonal to each other, but often they are not. So, the values of ϵ in figure 8 give us an indication of the average error in homography estimation for different out-of-plane rotations. In figure 8, we can see AKAZE has much higher ϵ values while the rest remained within a close range. This tells us AKAZE results in a much larger error in estimating the homography than the other methods.

We chose SIFT and SURF to evaluate how the execution time for detection scales up while increasing the number of objects. From table II, which shows the mean processing time for object detection, we can see that SURF had a detection time around 50% more than SIFT in all the cases. This

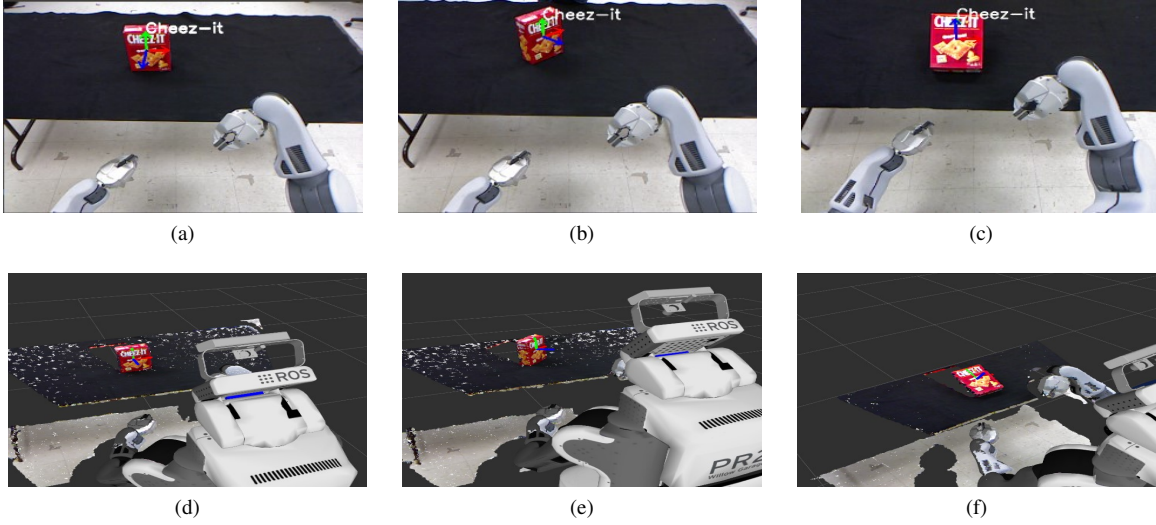


Fig. 5: (a),(b),(c) are recovered poses from robot's camera and (d),(e),(f) are corresponding poses visualized in RViz



Fig. 6: Pre-training canonical grasp

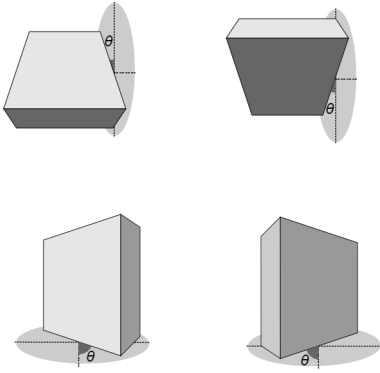


Fig. 7: Out of plane rotation

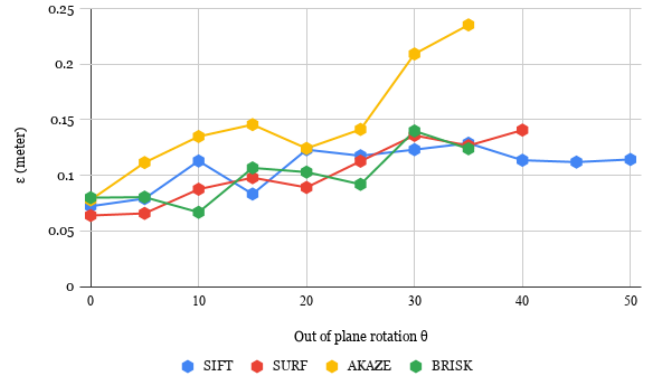


Fig. 8: Out of plane rotation vs ϵ

TABLE II: Execution time of SIFT and SURF for multiple object detection

Number of Objects	Detection time (second)	
	SIFT	SURF
1	0.06s	0.09s
2	0.11s	0.17s
3	0.17s	0.26s
4	0.22s	0.35s
5	0.28s	0.4s5
6	0.34s	0.54s

outcome coupled with the previous results prompted us to select SIFT for the subsequent experiments.

The system was capable of detecting multiple objects in real-time and at the same time could estimate their corresponding poses. Figure 9 shows detected objects with estimated directional planar vectors. We can also observe that the system was robust to in-plane rotation and partial occlusion.

We used RViz [71], a 3D visualizer for the Robot Operating System (ROS) [72], to validate the pose estimation. The

calculated directional axes were projected onto the image and the estimated poses were visualized in RViz. As shown in figure 5, we qualitatively verified the accuracy of the detection and the estimated pose by comparing the two outputs. We can see that both the outputs render similar results. We conducted experiments with multiple objects and human held objects as well. Figure 10 illustrates the simultaneous detection and pose estimation of two different boxes and an object held by a



Fig. 9: Multiple object detection with estimated planar vectors

human, respectively.



Fig. 10: (a) Pose estimation of multiple objects (b) Estimated pose of an object held by a human

$$\epsilon = \frac{1}{N} \sum_{i=1}^N \|\vec{x}_i' - \vec{x}_i\|, \text{ where } N \text{ is the number of frames} \quad (13)$$

B. Adaptive grasping

We assessed our approach for adaptive grasping keeping two different aspects of the robotic application in mind; robotic tasks that require 1) interacting with a static environment, and 2) interacting with humans.

We first tested our system for static objects where the object was attached to a tripod. Next, we set up experiments where the object was held by a human. We used a sticker book and a cartoon book and evaluated our system on a comprehensive set of poses. In almost all the experiments, the robot successfully grasped the object in a manner consistent with its training. There were some poses that were not reachable by the robot - for instance, when the object was pointing inward along the X-axis in the robot reference frame, it was not possible for the end-effector to make a top grasp. Figure 11 and 12 show the successful grasping of the robot for both types of experiments.

V. CONCLUSION AND FUTURE WORK

This work presents an approach that enables humanoid robots to grasp objects using planar pose estimation based on RGB image and depth data. We examined the performance of four feature-detector-descriptors for object recognition and found SIFT to be the best solution. We used FLANN's K-d Tree Nearest Neighbor implementation, and Bruteforce Hamming to find the keypoint matches and employed RANSAC to estimate the homography. The homography matrix was used to approximate the three orthonormal directional vectors on the planar object using perspective transformation. The pose of the



Fig. 11: Robot grasping an object from a tripod. Left: initial position of the robot's gripper, middle: gripper adapting to the object's pose, right: grasping of the object.

planar object was estimated from the three directional vectors. The system was able to detect multiple objects and estimate the pose of the objects in real-time. We also conducted experiments with the humanoid PR2 robot to show the practical applicability of the framework where the robot grasped objects by adapting to a range of different poses.

In the future, we plan to add GPU acceleration for the proposed algorithm that would further improve the overall computational efficiency of the system. We would like to extend the algorithm to automatically prioritize certain objects and limit the number of objects needed for detection based on different scheduled tasks. Finally, we would like to incorporate transferring grasp configuration for familiar objects and explore other feature matching technique e.g. multi probe LSH, hierarchical k-means tree, etc.

REFERENCES

- [1] K. He et al. Deep residual learning for image recognition. In *Proceedings of the IEEE conference on computer vision and pattern recognition*, pp. 770–778, 2016.
- [2] S. Liu and W. Deng. Very deep convolutional neural network based image classification using small training sample size. In *2015 3rd IAPR Asian Conference on Pattern Recognition (ACPR)*, pp. 730–734, 2015.
- [3] C. Szegedy et al. Going deeper with convolutions. In *Proceedings of the IEEE conference on computer vision and pattern recognition*, pp. 1–9, 2015.
- [4] D. C. Ciresan et al. Flexible, high performance convolutional neural networks for image classification. In *Twenty-Second International Joint Conference on Artificial Intelligence*, 2011.
- [5] P. Sermanet et al. Overfeat: Integrated recognition, localization and detection using convolutional networks. 2nd international conference



Fig. 12: Robot grasping an object held by a human. Left: initial position of the robot's gripper, middle: gripper adapting to the object's pose, right: grasping of the object.

on learning representations, iclr 2014. jan 2014. 2nd International Conference on Learning Representations, ICLR 2014 ; Conference date: 14-04-2014 Through 16-04-2014.

- [6] K. He et al. Spatial pyramid pooling in deep convolutional networks for visual recognition. *IEEE transactions on pattern analysis and machine intelligence*, 37(9):1904–1916, 2015.
- [7] R. Girshick. Fast R-CNN. In *Proceedings of the IEEE international conference on computer vision*, pp. 1440–1448, 2015.
- [8] S. Ren et al. Faster R-CNN: towards real-time object detection with region proposal networks. In *Advances in neural information processing systems*, pp. 91–99, 2015.
- [9] W. Liu et al. Ssd: Single shot multibox detector. In *European conference on computer vision*, pp. 21–37. Springer, 2016.
- [10] J. Redmon et al. You only look once: Unified, real-time object detection. In *Proceedings of the IEEE conference on computer vision and pattern recognition*, pp. 779–788, 2016.
- [11] J. Redmon and A. Farhadi. Yolo9000: better, faster, stronger. In *Proceedings of the IEEE conference on computer vision and pattern recognition*, pp. 7263–7271, 2017.
- [12] T.-Y. Lin et al. Focal loss for dense object detection. In *Proceedings of the IEEE international conference on computer vision*, pp. 2980–2988, 2017.
- [13] V. Badrinarayanan et al. Segnet: A deep convolutional encoder-decoder architecture for image segmentation. *IEEE transactions on pattern analysis and machine intelligence*, 39(12):2481–2495, 2017.
- [14] K. He et al. Mask r-cnn. In *Proceedings of the IEEE international conference on computer vision*, pp. 2961–2969, 2017.
- [15] O. Ronneberger et al. U-net: Convolutional networks for biomedical image segmentation. In *International Conference on Medical image computing and computer-assisted intervention*, pp. 234–241. Springer, 2015.
- [16] D. J. Butler et al. A naturalistic open source movie for optical flow evaluation. In A. Fitzgibbon et al., editors, *Computer Vision – ECCV 2012*, pp. 611–625, Berlin, Heidelberg, 2012. Springer Berlin Heidelberg.
- [17] N. Mayer et al. A large dataset to train convolutional networks for disparity, optical flow, and scene flow estimation. In *Proceedings of the IEEE Conference on Computer Vision and Pattern Recognition*, pp. 4040–4048, 2016.
- [18] W. Qiu and A. Yuille. Unrealcv: Connecting computer vision to unreal engine. In *European Conference on Computer Vision*, pp. 909–916. Springer, 2016.
- [19] Y. Zhang et al. Unrealstereo: A synthetic dataset for analyzing stereo vision. *arXiv preprint arXiv:1612.04647*, 2016.
- [20] J. McCormac et al. Scenenet rgb-d: Can 5m synthetic images beat generic imagenet pre-training on indoor segmentation? In *The IEEE International Conference on Computer Vision (ICCV)*, Oct 2017.
- [21] Y. Xiang et al. Posecnn: A convolutional neural network for 6d object pose estimation in cluttered scenes. In *Robotics: Science and Systems (RSS)*, 2018.
- [22] J. Tremblay et al. Deep object pose estimation for semantic robotic grasping of household objects. In *Conference on Robot Learning (CoRL)*, 2018.
- [23] E. Brachmann et al. Learning 6d object pose estimation using 3d object coordinates. In *European conference on computer vision*, pp. 536–551. Springer, 2014.
- [24] C. Wang et al. Densefusion: 6d object pose estimation by iterative dense fusion. In *Proceedings of the IEEE Conference on Computer Vision and Pattern Recognition*, pp. 3343–3352, 2019.
- [25] Y. Hu et al. Segmentation-driven 6d object pose estimation. In *Proceedings of the IEEE Conference on Computer Vision and Pattern Recognition*, pp. 3385–3394, 2019.
- [26] C. G. Harris et al. A combined corner and edge detector. In *Alvey vision conference*, volume 15, pp. 10–5244. Citeseer, 1988.
- [27] C. Tomasi and T. Kanade. Detection and tracking of point features. *School of Computer Science, Carnegie Mellon Univ. Pittsburgh*, 1991.
- [28] J. Shi et al. Good features to track. In *1994 Proceedings of IEEE conference on computer vision and pattern recognition*, pp. 593–600. IEEE, 1994.
- [29] D. Hall et al. Saliency of interest points under scale changes. In *BMVC*, pp. 1–10, 2002.
- [30] T. Lindeberg. Feature detection with automatic scale selection. *International journal of computer vision*, 30(2):79–116, 1998.
- [31] K. Mikolajczyk and C. Schmid. Indexing based on scale invariant interest points. In *Proceedings Eighth IEEE International Conference on Computer Vision. ICCV 2001*, volume 1, pp. 525–531. IEEE, 2001.
- [32] D. G. Lowe. Distinctive image features from scale-invariant keypoints. *International Journal of Computer Vision*, 2004.
- [33] H. Bay et al. Surf: Speeded up robust features. In A. Leonardis et al., editors, *Computer Vision – ECCV 2006*, pp. 404–417, Berlin, Heidelberg, 2006. Springer Berlin Heidelberg.
- [34] Y. Ke and R. Sukthankar. Pca-sift: A more distinctive representation for local image descriptors. In *Proceedings of the 2004 IEEE Computer Society Conference on Computer Vision and Pattern Recognition, 2004. CVPR 2004.*, volume 2, pp. II–II. IEEE, 2004.
- [35] S. K. Lodha and Y. Xiao. Gsift: geometric scale invariant feature transform for terrain data. In *Vision Geometry XIV*, volume 6066, pp. 60660L. International Society for Optics and Photonics, 2006.
- [36] A. E. Abdel-Hakim and A. A. Farag. Csift: A sift descriptor with color invariant characteristics. In *2006 IEEE computer society conference on computer vision and pattern recognition (CVPR'06)*, volume 2, pp. 1978–1983. Ieee, 2006.
- [37] J.-M. Morel and G. Yu. Asift: A new framework for fully affine invariant image comparison. *SIAM journal on imaging sciences*, 2(2):438–469, 2009.
- [38] P. F. Alcantarilla et al. Gauge-surf descriptors. *Image and vision computing*, 31(1):103–116, 2013.
- [39] T.-K. Kang et al. Mdghm-surf: A robust local image descriptor based on modified discrete gaussian–hermite moment. *Pattern Recognition*, 48(3):670–684, 2015.
- [40] J. Fu et al. C-surf: Colored speeded up robust features. In *International Conference on Trustworthy Computing and Services*, pp. 203–210. Springer, 2012.
- [41] E. Rosten and T. Drummond. Machine learning for high-speed corner detection. In *European conference on computer vision*, pp. 430–443.

- Springer, 2006.
- [42] E. Mair et al. Adaptive and generic corner detection based on the accelerated segment test. In *European conference on Computer vision*, pp. 183–196. Springer, 2010.
 - [43] M. Calonder et al. Brief: Computing a local binary descriptor very fast. *IEEE transactions on pattern analysis and machine intelligence*, 34(7):1281–1298, 2011.
 - [44] E. Rublee et al. Orb: An efficient alternative to sift or surf. In *2011 International Conference on Computer Vision*, pp. 2564–2571, Nov 2011.
 - [45] S. Leutenegger et al. Brisk: Binary robust invariant scalable keypoints. In *2011 International conference on computer vision*, pp. 2548–2555. Ieee, 2011.
 - [46] R. Ortiz. Freak: Fast retina keypoint. In *Proceedings of the 2012 IEEE Conference on Computer Vision and Pattern Recognition (CVPR)*, CVPR '12, pp. 510–517, Washington, DC, USA, 2012. IEEE Computer Society.
 - [47] P. F. Alcantarilla et al. Kaze features. In A. Fitzgibbon et al., editors, *Computer Vision – ECCV 2012*, pp. 214–227, Berlin, Heidelberg, 2012. Springer Berlin Heidelberg.
 - [48] P. F. Alcantarilla et al. Fast explicit diffusion for accelerated features in nonlinear scale spaces. In *British Machine Vision Conf. (BMVC)*, 2013.
 - [49] J. Weickert et al. Cyclic schemes for pde-based image analysis. *International Journal of Computer Vision*, 118(3):275–299, 2016.
 - [50] S. Grewenig et al. From box filtering to fast explicit diffusion. In *Joint Pattern Recognition Symposium*, pp. 533–542. Springer, 2010.
 - [51] G. Simon and M. . Berger. Pose estimation for planar structures. *IEEE Computer Graphics and Applications*, 22(6):46–53, Nov 2002.
 - [52] Changhai Xu et al. 3d pose estimation for planes. In *2009 IEEE 12th International Conference on Computer Vision Workshops, ICCV Workshops*, pp. 673–680, Sep. 2009.
 - [53] M. Donoser et al. Robust planar target tracking and pose estimation from a single concavity. In *2011 10th IEEE International Symposium on Mixed and Augmented Reality*, pp. 9–15, Oct 2011.
 - [54] D. Nistér and H. Stewénus. Linear time maximally stable extremal regions. In D. Forsyth et al., editors, *Computer Vision – ECCV 2008*, pp. 183–196, Berlin, Heidelberg, 2008. Springer Berlin Heidelberg.
 - [55] A. Sahbani et al. An overview of 3d object grasp synthesis algorithms. *Robotics and Autonomous Systems*, 60(3):326–336, 2012.
 - [56] J. Bohg et al. Data-driven grasp synthesis—a survey. *IEEE Transactions on Robotics*, 30(2):289–309, 2013.
 - [57] B. Kehoe et al. Cloud-based robot grasping with the google object recognition engine. In *2013 IEEE International Conference on Robotics and Automation*. IEEE, May 2013.
 - [58] K. Huebner et al. Minimum volume bounding box decomposition for shape approximation in robot grasping. In *2008 IEEE International Conference on Robotics and Automation*. IEEE, May 2008.
 - [59] S. Caldera et al. Review of deep learning methods in robotic grasp detection. *Multimodal Technologies and Interaction*, 2(3):57, 2018.
 - [60] J. Yu et al. A vision-based robotic grasping system using deep learning for 3d object recognition and pose estimation. In *2013 IEEE International Conference on Robotics and Biomimetics (ROBIO)*. IEEE, December 2013.
 - [61] O. Kroemer et al. Active learning using mean shift optimization for robot grasping. In *2009 IEEE/RSJ International Conference on Intelligent Robots and Systems*. IEEE, October 2009.
 - [62] J. Aleotti and S. Caselli. Part-based robot grasp planning from human demonstration. In *2011 IEEE International Conference on Robotics and Automation*. IEEE, May 2011.
 - [63] A. Saxena et al. Robotic grasping of novel objects using vision. *The International Journal of Robotics Research*, 27(2):157–173, February 2008.
 - [64] L. Montesano and M. Lopes. Active learning of visual descriptors for grasping using non-parametric smoothed beta distributions. *Robotics and Autonomous Systems*, 60(3):452–462, March 2012.
 - [65] J. Nogueira et al. Unscented bayesian optimization for safe robot grasping. In *2016 IEEE/RSJ International Conference on Intelligent Robots and Systems (IROS)*. IEEE, October 2016.
 - [66] O. Andersson and S. Reyna Marquez. A comparison of object detection algorithms using unmanipulated testing images: Comparing sift, kaze, akaze and orb, 2016.
 - [67] E. Karami et al. Image matching using sift, surf, brief and orb: performance comparison for distorted images. *The 24th Annual Newfoundland Electrical and Computer Engineering Conference, NECEC*, 2015.
 - [68] S. A. K. Tareen and Z. Saleem. A comparative analysis of sift, surf, kaze, akaze, orb, and brisk. In *2018 International conference on computing, mathematics and engineering technologies (iCoMET)*, pp. 1–10. IEEE, 2018.
 - [69] M. Muja and D. G. Lowe. Fast approximate nearest neighbors with automatic algorithm configuration. In *International Conference on Computer Vision Theory and Application VISSAPP'09*, pp. 331–340. INSTICC Press, 2009.
 - [70] M. A. Fischler and R. C. Bolles. Random sample consensus: A paradigm for model fitting with applications to image analysis and automated cartography. *Commun. ACM*, 24(6):381–395, June 1981.
 - [71] David Gossow, Chad Rockey, Kei Okada, Julius Kammerl, Acorn Pooley, Rein Appeldoorn, Robert Haschke. Rviz.
 - [72] Stanford Artificial Intelligence Laboratory et al. Robotic operating system.